ACS OMEGA

http://pubs.acs.org/journal/acsodf

Article

Influence of Torrefaction on Biomass Devolatilization

Federica Barontini,* Enrico Biagini, and Leonardo Tognotti

Cite This: *ACS Omega* 2021, 6, 20264−20278

Read Online

ACCESS | Metrics & More | Article Recommendations

ABSTRACT: The present study investigated the effect of torrefaction on the devolatilization characteristics of three lignocellulosic biomass feedstocks with different degrees of torrefaction together with their parent fuel, palm kernel shell, a residue of palm oil production. Thermogravimetric (TG) analysis was employed for the study of the devolatilization process. A kinetic model based on three parallel reactions corresponding to biomass chemical components was applied to TG data and used for the evaluation of reaction kinetics. The results obtained indicated that the torrefaction process led to a significant reduction of the hemicellulose content of the investigated biofuels. The characterization of volatile products evolved during biofuel devolatilization was performed by TG analysis coupled with Fourier transform infrared spectroscopy. The emission characteristics and the yields of the main volatile products were assessed. Specific linear correlations between volatile yields and the torrefaction degree could be observed.

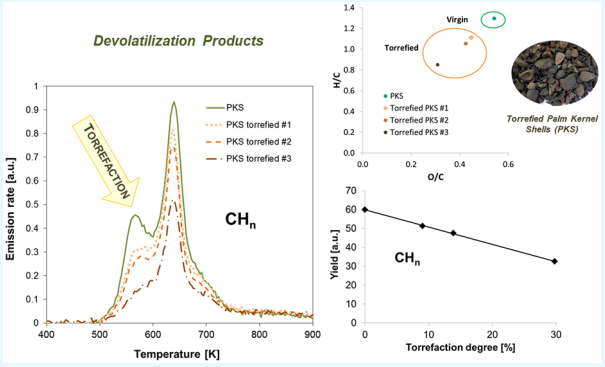

1. INTRODUCTION

With increasing concerns on the depletion of conventional energy resources such as fossil fuels, dependence on foreign energy sources, and environmental threats such as air pollution, global warming, and climate change, the development of renewable, sustainable, and environmentally friendly energy resources has become an important topic. Among the available renewable energy resources, biomass appears as one of the most promising resources, because of its abundance, wide distribution, carbon dioxide neutrality, and low emissions of pollutants (i.e., sulfur dioxide and nitrogen oxides).

Thermochemical conversion processes such as combustion, gasification, and pyrolysis are promising routes to convert biomass to heat, power, fuels, and chemicals. However, the use of raw biomass feedstock has several drawbacks, due to biomass inherent characteristics. These include low bulk density, hygroscopic character, high moisture content, high oxygen content resulting in a relatively low heating value (LHV), low energy density, fibrous nature, and heterogeneous composition. For instance, the high moisture content further decreases its heating value and could provide storage complications such as self-heating due to chemical oxidation and microbial activity. The low energy density results in onerous handling and transportation. The fibrous nature gives rise to grinding and feeding difficulties.

Therefore, in order to overcome the aforementioned limitations, a pretreatment process is often necessary to improve biomass properties. Among the proposed technologies, torrefaction has attracted noticeable interest in the last two decades. It is a mild thermal treatment carried out at temperatures ranging from 200 to 300 °C for a residence time of few minutes to 1 h in an inert atmosphere at atmospheric pressure.[1] Torrefaction is a promising technology to upgrade lignocellulosic biomass to a high-quality bioenergy carrier. Compared with the untreated biomass, the torrefied product is characterized in reduced moisture content, lower O/C and H/C ratios, higher energy density, improved grindability and homogeneity, increased hydrophobic character, and reduced risk of biological degradation and self-ignition.[1−5] After torrefaction, a higher quality product with properties similar to those of coal is obtained.

Most of the published research studies have focused on the effect of torrefaction operating conditions such as temperature and residence time on the yield and fuel properties of the torrefied products. Torrefaction studies have largely been performed on woody and herbaceous biomass, including bamboo, beech, birch, eucalyptus, larch, pine, oak, willow, Miscanthus, and reed canary grass.[2] The torrefaction of different agricultural residues was also examined in the literature, such as almond shells,[6] arecanut husk,[7] coffee residues,[8] corncobs,[9] cotton stalk,[10] rape stalk,[11] rice

Received: April 22, 2021
Accepted: June 7, 2021
Published: July 28, 2021

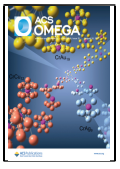

husk,[8,12,13] rice straw,[10,11] wheat straw,[14,15] sugar cane bagasse,[16] olive wastes,[17,18] and oil palm wastes.[19−28]

Torrefied biomass is an attractive source of fuel for combustion and gasification systems because of its enhanced fuel quality in terms of bulk density and heating value, which potentially improves the thermal efficiencies, compared to using raw biomass. Furthermore, the increased energy density and grindability lead to a reduction in energy requirements for transportation and grinding. Pulverized fuel combustion in coal-fired electrical or thermal power plants and entrained flow gasification are the most promising applications.[29] Some researchers investigated the performance of torrefied biomass in gasification.[30−36] It was generally concluded that torrefied fuels may offer benefits as feedstock for gasification, in particular, in terms of improved syngas quality, increased syngas yield, and reduced tar production. Besides, recent studies examined the effect of a torrefaction pretreatment on the pyrolysis process of different biomass feedstocks, and the results showed that torrefaction is an effective method for improving the quality of the produced bio-oil.[7,37]

Pyrolysis plays an important role because it is not only a bio-oil production method but it is also the first step in either gasification or combustion. Therefore, a fundamental understanding of pyrolysis (or devolatilization) is essential for the design, operation, and optimization of thermochemical conversion systems. Devolatilization kinetics and volatile speciation are the basic information required. While many efforts have been devoted to investigating the pyrolysis of different biomasses, kinetic parameters and volatile speciation for the pyrolysis of torrefied fuels have been barely reported. Recent investigations examined the devolatilization of torrefied fuels by thermogravimetric (TG) analysis.[9,15,26,38−42] Key devolatilization parameters, including initial temperature, maximum weight loss rate and its corresponding temperature, and final residue mass, were obtained from the TG data.[9,15,26,38−42] Further elaboration of the TG data was carried out for the evaluation of the reaction kinetic parameters in a few studies.[9,26,39−42] A deep insight into the effect of torrefaction on the kinetics of biofuel pyrolysis is still required. Furthermore, to the best of our knowledge, no studies focused on how torrefaction affects the yields of the main volatile species evolved in the pyrolysis process.

In the present work, the devolatilization of three samples with different degrees of torrefaction together with their parent biomass was studied. The key objective of the study was to investigate the effect of torrefaction on biomass pyrolysis characteristics, including kinetics and quantities of volatile products evolved, in order to increase the understanding of the pyrolysis of torrefied biomass and provide basic information for the design and operation of thermochemical conversion units using torrefied feedstocks.

The studied biomass material is the palm kernel shell (PKS). The PKS is a solid residue generated as a byproduct of palm oil production. In recent years, the abundance of palm oil waste has been increasing with the fast development of palm oil industries especially in Southeast Asia, that is, Malaysia, Indonesia, and Thailand. Based on the latest statistics, about 4.85 million tonnes of PKS were produced from the processing of fresh fruit bunches in palm oil mills in Malaysia in 2018.[43] The PKS is an attractive biomass source for bioenergy production. As a matter of fact, production of biofuels from lignocellulosic biowaste by thermochemical conversion helps to achieve the dual objectives of waste management and energy and chemical recovery. Currently, the PKS is primarily used in low-efficiency direct-fired boiler systems to generate steam in palm oil processing plants.[24,44] Several researchers are focusing on PKS torrefaction, and some of the promising results were recently highlighted, especially in terms of the increased heating value and better grindability of the torrefied fuel.[19−21,23,24,27] Hence, further investigations on the reactivity of torrefied PKS are recommended.

2. MATERIALS AND METHODS

2.1. Materials. Torrefied samples were obtained from torrefaction of PKS at increasing severity degrees, that is, at temperatures of 473, 523, and 573 K, with a residence time of 30 min, and were classified as torrefied PKS #1, torrefied PKS #2, and torrefied PKS #3, respectively. Temperatures ranging from 473 to 573 K are commonly used in torrefaction pretreatments, and torrefaction times typically range from 10 to 60 min (see the Introduction section and references cited therein). A residence time of 30 min was thus selected since it represented a common and average value employed in torrefaction processes. Indeed, a 30 min torrefaction residence time was reported in several studies related to torrefied agricultural residues, for example, arecanut husk,[7] corncobs,[9] rape stalk,[11] rice husk,[13,33] rice straw,[11] wheat straw,[15] olive kernels,[36] PKS,[21] and oil palm fiber pellets.[22]

Each material was milled and sieved in the size fraction 90−150 μm. The proximate analysis (i.e., moisture, volatile matter, VM, fixed carbon, FC, and ash content), the ultimate analysis (carbon, hydrogen, nitrogen, and sulfur content), and the higher and lower heating value (HHV and LHV) of all materials are listed in Table 1. Biofuel samples were dried at 378 K until constant in mass before every experimental run.

The torrefaction degree was defined as the reduction of the volatile content upon torrefaction divided by the initial volatile content of the raw material (eq 1)[45]

$$\text{torrefaction degree (\%)} = 100\left(1 - \frac{\text{VM}_{\text{torr}}^{\text{daf}}}{\text{VM}_{\text{raw}}^{\text{daf}}}\right) \quad (1)$$

where $\text{VM}_{\text{torr}}^{\text{daf}}$ and $\text{VM}_{\text{raw}}^{\text{daf}}$ are the VM content on a dry and ash-free basis of the torrefied and raw material, respectively. A torrefaction degree of 9.0, 13.9, and 29.8% was calculated for torrefied PKS #1, #2, and #3 samples, respectively.

2.2. Experimental Techniques and Procedures. Biofuel characterization, including proximate analysis, ultimate analysis, and heating value determination, was carried out according to standard procedures. The test methods and the instruments used are summarized in Table 2.

TG analysis was employed for the study of the devolatilization process. TG data were obtained using a TA Instruments Q-500 thermobalance. Constant heating rate runs were performed from 378 to 1173 K, with a purge gas flow (100 mL/min) of pure nitrogen. Different heating rates were used in the experimental runs: 5, 10, 20, and 40 K/min. Samples of around 5 mg were used for each test to limit the thermal gradients in the conditions used.

Differential scanning calorimetry (DSC) data were obtained using a Mettler DSC 25 calorimeter. Constant heating rate (20 K/min) runs were performed from 348 to 823 K, with a purge gas flow (300 mL/min) of pure nitrogen. The DSC runs were performed using aluminum crucibles without a lid (thus resulting in a 5 mm-diameter surface available for mass transfer to the gas flow) or with a pierced lid (thus limiting the surface

https://doi.org/10.1021/acsomega.1c02141
ACS Omega 2021, 6, 20264−20278

Table 1. Proximate Analysis, Ultimate Analysis, and Heating Value of the Investigated Biofuels (ar: As-Received; daf: Dry Ash-Free)

biofuel	moisture [%, ar]	VM [%, dry]	FC [%, dry]	ash [%, dry]	C [%, daf]	H [%, daf]	N [%, daf]	S [%, daf]	O [%, daf]	HHV [MJ/kg, dry]	LHV [MJ/kg, dry]
PKS	7.40	75.17	18.32	6.51	54.43	5.92	0.40	0.04	39.21	20.42	19.28
torrefied PKS #1	5.43	67.44	24.77	7.79	58.89	5.50	0.54	0.04	35.03	21.31	20.26
torrefied PKS #2	5.78	63.80	28.35	7.85	60.13	5.32	0.54	0.04	33.97	21.68	20.66
torrefied PKS #3	5.24	51.10	39.39	9.51	67.05	4.78	0.63	0.04	27.50	23.44	22.55

Table 2. Test Methods and Instruments Used for Biofuel Characterization

parameter	test method	instrument
moisture	EN ISO 18134-2:2017	Binder oven
VM, FC and ash content	ASTM E1131-20	TA instruments TGA Q500 TG analyzer
C, H, N content	EN ISO 16948:2015	LECO TruSpec CHN elemental analyzer
S content	ISO 19579:2006	LECO SC-132 sulfur analyzer
heating value	EN ISO 18125:2017	LECO AC-500 isoperibol calorimeter

available for mass transfer to a 1 mm-diameter hole). Typical sample weights of 5 mg were used. The char formed in DSC runs was weighted, and a second run was performed on the char sample using the same experimental conditions. All the DSC results were corrected by baselines obtained from runs with empty crucibles. The heat flow curves due to the thermal effects of the pyrolysis reaction were obtained from the experimental heat flow curves following the procedures extensively described elsewhere.[46] The heat of pyrolysis was calculated from a numerical integration of the heat flow curves.

The volatile products of the pyrolysis process were investigated using TG analysis coupled with Fourier transformed infrared (TG-FTIR) spectroscopy of evolved gases. TG-FTIR simultaneous measurements for the online analysis of volatile compounds formed during devolatilization runs were carried out by coupling a Bruker Equinox 55 FTIR spectrometer to a Netzsch STA 409/C thermoanalyzer using a 2 mm internal diameter Teflon tube. The transfer line and the head of the TG balance were heated at a constant temperature of 483 K to limit the condensation of volatile products. FTIR measurements were carried out in a specifically developed gas cell heated at a constant temperature of 523 K. A constant heating rate of 20 K/min was used in the experimental runs from 378 to 1273 K. Experimental runs were carried out using a purge gas flow (60 mL/min) of pure nitrogen. A residence time of 30 s in the transfer line could be evaluated for the evolved gases, and this value was assumed as the time delay correction to be used for the comparison of TG and FTIR results. FTIR spectra were collected at 4 cm^{-1} resolution, with coaddition of 16 scans per spectrum. This resulted in a temporal resolution of 9.5 s, which was sufficient to follow the gas evolution rate characteristic of TG runs at heating rates of 20 K/min. Typical sample weights of 15 mg were employed. Each test was replicated at least twice.

2.3. Kinetic Analysis. The TG data were used to calculate the conversion degree (α) of the biofuel in the devolatilization reaction

$$\alpha = \frac{w_0 - w}{w_0 - w_\infty} \quad (2)$$

where w is the actual mass of the sample registered by the TG balance and w_0 and w_∞ are the initial and final mass, respectively (the initial mass was taken at 400 K, so that any residual moisture was completely removed from the sample).

Biomass devolatilization is a very complex process, which proceeds through a complex network of reactions. A large number of modeling approaches and methods have been proposed in the literature for analyzing the kinetics of biomass pyrolysis.[47] An approach based on chemical components, which has proved to be able to describe with a good accuracy

https://doi.org/10.1021/acsomega.1c02141
ACS Omega 2021, 6, 20264−20278

the thermal decomposition behavior of a wide variety of lignocellulosic substrates,[41,48−59] was selected in the present study to model devolatilization kinetics.

It is based on the commonly accepted assumption that the behavior of a lignocellulosic biomass can be predicted by a weighted sum of the behavior of the chemical components, namely, cellulose, hemicellulose, and lignin. It is also assumed that these components react independently with negligible influence due to their interactions, so the devolatilization of the biomass can be represented by a set of parallel reactions.

The conversion of the i-th biomass can thus be expressed as

$$\alpha_i = \sum_{j=1}^{3} x_{i,j}\alpha_j \tag{3}$$

where $x_{i,j}$ is the mass fraction of the j-th component in the i-th biomass and α_j is the conversion of the j-th component, with the constraint

$$\sum_{j=1}^{3} x_{i,j} = 1, \qquad \forall\ i \tag{4}$$

The relation can be also expressed in terms of the conversion rate $d\alpha/dt$

$$\frac{d\alpha_i}{dt} = \sum_{j=1}^{3} x_{i,j}\frac{d\alpha_j}{dt} \tag{5}$$

According to literature studies,[41,48−59] the devolatilization of the j-th component can be described by a single-step n-order reaction model with the rate constant following the Arrhenius law

$$\frac{d\alpha_j}{dt} = A_j e^{-E_j/RT}(1-\alpha_j)^{n_j} \tag{6}$$

where A_j is the pre-exponential factor, E_j is the activation energy, n_j is the reaction order, R is the universal gas constant, and T is the absolute temperature.

Antal and Varhegyi[60] suggested that cellulose pyrolysis can be accurately described by a single-step, first-order kinetic model, and a general consensus exists in the literature on a first-order reaction model for cellulose devolatilization kinetics.[41,48−58] Indeed, most studies show that the assumption of a single-step, first-order reaction process for each of the three components in the proposed summative model for the devolatilization of biomass samples is able to reproduce the experimental results satisfactorily.[41,48−50,56−58]

Nevertheless, different values of the reaction order can be found in the literature, especially for the lignin component[51−53,55] (some studies indicate a third-order reaction rate law for the pyrolysis of lignin[51−53]). Slightly better agreement between simulated and experimental data was reported for summative three-component models with n-order kinetics.[54,55] Anyway, the use of the three first-order parallel reaction model was suggested, since its accuracy to represent biomass pyrolysis is high enough, and it is more realistic with respect to the chemical interpretation of the reaction order.[54] Although it can be expected that the introduction of a higher number of fitting parameters, such as the values of the reaction orders for the components, or the introduction of multiple steps in the devolatilization mechanism would improve the accuracy of the model, a simple model with few kinetic parameters is often required in engineering applications.[50,61]

Thus, biofuel pyrolysis was modeled by a kinetic scheme (named the cellulose hemicellulose lignin (CHL) model in the following) consisting of three parallel reactions for cellulose, hemicellulose, and lignin, and a single-step first-order reaction model (n = 1) was assumed for the devolatilization of each component

$$\frac{d\alpha_j}{dt} = A_j e^{-E_j/RT}(1-\alpha_j) \tag{7}$$

The approximation of Coats and Redfern[62] was assumed to analytically solve the single differential eq 7

$$\ln\left[\frac{-\ln(1-\alpha_j)}{T^2}\right] = \ln\left[\frac{A_j R}{bE_j}\cdot\left(1-\frac{2RT}{E_j}\right)\right] - \frac{E_j}{RT} \tag{8}$$

where b is the heating rate used during the experimental test.

The values of the unknown parameters (E_j and A_j for the components and the mass fractions for the chemical composition) were obtained by an optimization procedure which was carried out according to the method described in the work of Biagini and Tognotti,[58] with the data set formed of the tests at the four heating rates for all materials. The parameters E_j and A_j for the chemical components were the same for all materials, while the chemical composition was specific for each material.

2.4. Evolved Gas Analysis. Gas evolution profiles of volatile species released in TG-FTIR runs were obtained from the experimental data following a specific procedure. The procedure used an integral form of the Lambert−Beer law over a selected wavenumber interval characteristic for the species of interest, free of additional contributions from other substances

$$I = \int_{\tilde{\nu}_1}^{\tilde{\nu}_2} \mathcal{A}(\tilde{\nu})d\tilde{\nu} = c\int_{\tilde{\nu}_1}^{\tilde{\nu}_2} \varepsilon(\tilde{\nu})l\,d\tilde{\nu} = Kc \tag{9}$$

where $\mathcal{A}$ is the measured absorbance, I is the integral value, $\tilde{\nu}$ is the wavenumber, ε is the molar extinction coefficient of the gaseous compound, l is the optical path length used in the measurement, c is the concentration, ($\tilde{\nu}_1$, $\tilde{\nu}_2$) is the wavenumber interval selected for the measurement, and K is a constant.

The simultaneous formation of a wide number of volatile compounds complicated the selection of such intervals. During biomass devolatilization, specific compounds (namely, CO_2, CO, H_2O, CH_4, CH_3OH, and HCOOH) could be easily detected, while organic compounds were grouped in the following classes: compounds with a characteristic C−H bond were classified in the hydrocarbon group and compounds with characteristic C═O bond typical of aldehydes, ketones, carboxylic acids, and esters were classified in the carbonyl compound group. The following wavenumber intervals were selected for the different species: 2240−2400 cm^{-1} for CO_2, 2143−2236 cm^{-1} for CO, 3792−4025 cm^{-1} for H_2O, 3001−3026 cm^{-1} for CH_4, 1026−1040 cm^{-1} for CH_3OH, 1101−1111 cm^{-1} for HCOOH, 2645−3042 cm^{-1} for hydrocarbon compounds, and 1660−1838 cm^{-1} for carbonyl compounds. TG-FTIR measurements were thus used to generate specific gas profiles to qualitatively monitor the evolution of a species as a function of the time (or temperature) of the TG furnace.

Specific data on the total quantities of the different products evolved in TG-FTIR runs could be obtained by integration of eq 9 with respect to time

https://doi.org/10.1021/acsomega.1c02141
ACS Omega 2021, 6, 20264−20278

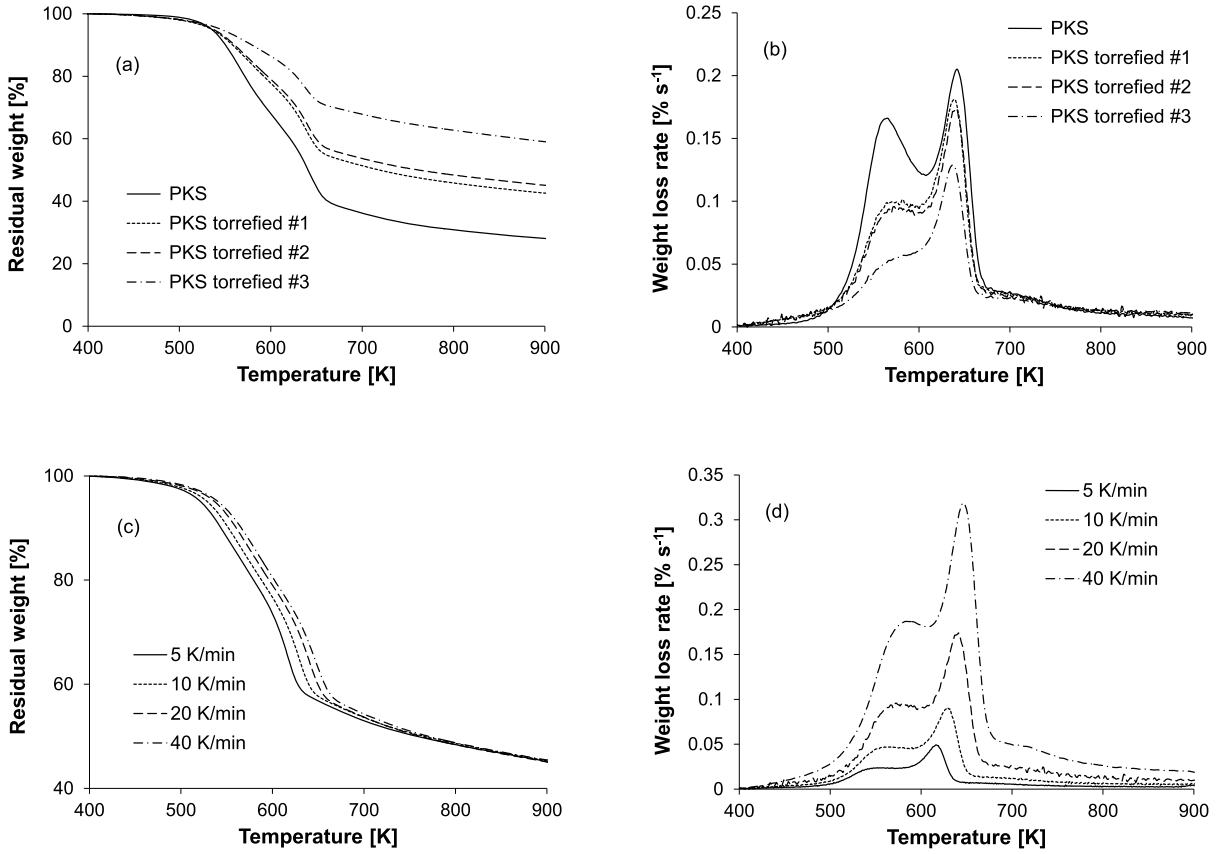

Figure 1. Results of TG runs for raw and torrefied PKS: weight loss (a) and weight loss rate (b) curves at the 20 K/min heating rate for PKS with different torrefaction degrees and weight loss (c) and weight loss rate (d) curves at different heating rates for torrefied PKS #2.

$$D = \int_{t_1}^{t_2} \left[\int_{\tilde{\nu}_1}^{\tilde{\nu}_2} \mathcal{A}(\tilde{\nu}) \mathrm{d}\tilde{\nu} \right] \mathrm{d}t = \int_{t_1}^{t_2} Kc \mathrm{d}t = K'm \tag{10}$$

The value of integral (D) is directly related to the total amount (m) of the species of interest evolved during the (t_1, t_2) interval.

Quantitative results were obtained for CO_2, CO, and H_2O, by the use of calibration data. A gas-pulse calibration method[63] was used for CO_2 and CO: known quantities of the gaseous compound were sent to the IR measurement cell using a gas injection system consisting of a rotary sample valve allowing a carrier gas to purge a known-volume loop, previously filled with a calibration gas of known composition. A vaporization-based calibration method[63] was employed for H_2O: TG-FTIR calibration runs were performed by vaporizing the compound in the TG analyzer, the use of pure water samples of different weights allowing the vaporization of different quantities of water, which were carried to the FTIR measurement cell by the carrier gas flow.

3. RESULTS AND DISCUSSION

3.1. Devolatilization Behavior: Results of TG and DSC Runs. The main characteristics of raw and torrefied PKS samples are summarized in Table 1. As expected, increasing the torrefaction temperature led to biofuels with decreased H/C and O/C values and increased heating value. The H/C atomic ratio decreased from 1.11 to 0.85, and the O/C atomic ratio decreased from 0.45 to 0.31 for the torrefied samples #1 and #3, respectively, while the corresponding values for the raw biomass were 1.30 and 0.54, respectively. The LHV increased from 19.28 for the raw biomass to 22.55 MJ/kg for PKS #3 (Table 1). Although the torrefaction pretreatment significantly improved the biomass energy density, the energy consumption for the torrefaction process had to be considered. Li et al.[64] evaluated the heat consumption for PKS torrefaction, for process temperatures ranging from 473 to 573 K and a residence time of 30 min. The energy requirement for PKS torrefaction varied from 0.18 MJ/kg at a process temperature of 473 K to 0.39 MJ/kg at 573 K. Therefore, it could be inferred that the increase in calorific value was considerably higher than the heat consumed for torrefaction.

TG analysis provided useful data related to the devolatilization behavior of the selected samples. Typical results of TG runs are shown in Figure 1.

Figure 1a reports the TG curves obtained for raw and torrefied samples using a heating rate of 20 K/min. As expected, the amount of released volatiles decreased with the increased torrefaction degree (Figure 1a). The derivative TG (dTG) curves (Figure 1b) revealed a composite shape due to the devolatilization of the different chemical components of biomass, namely, hemicellulose, cellulose, and lignin.[65] The first peak of the dTG curve (with a peak temperature of about 565 K for the 20 K/min heating rate) could be ascribed to the decomposition of hemicellulose, which was the most reactive component, while the main devolatilization peak (with a peak temperature of about 640 K) corresponded to cellulose decomposition. Lignin decomposed in a wider temperature range, and this hindered the appearance of a distinct peak related to this component. Finally, a long tail of devolatilization

https://doi.org/10.1021/acsomega.1c02141
ACS Omega 2021, 6, 20264−20278

Table 3. Devolatilization Parameters of the Investigated Biofuels for Different Values of Heating Rate (T_{onset}: Onset Temperature, Correspondent to a Conversion Degree of 0.05; T_{max}: Temperature at the Maximum Weight Loss Rate; dTG_{max}: Maximum Weight Loss Rate)

	b = 5 K/min			b = 10 K/min			b = 20 K/min			b = 40 K/min		
biofuel	T_{onset} [K]	T_{max} [K]	dTG_{max} [%/s]	T_{onset} [K]	T_{max} [K]	dTG_{max} [%/s]	T_{onset} [K]	T_{max} [K]	dTG_{max} [%/s]	T_{onset} [K]	T_{max} [K]	dTG_{max} [%/s]
PKS	520	619	0.0587	529	632	0.110	533	642	0.205	537	646	0.393
Torrefied #1	524	616	0.0513	532	630	0.0977	540	640	0.181	540	643	0.348
Torrefied #2	526	617	0.0491	533	629	0.0907	542	641	0.174	548	647	0.319
Torrefied #3	543	619	0.0362	548	629	0.0680	559	640	0.126	558	646	0.246

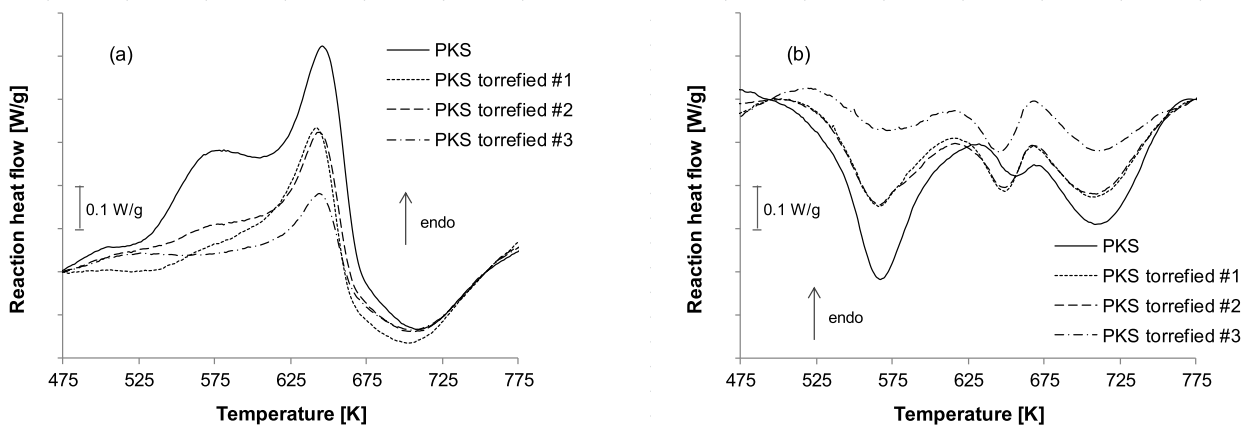

Figure 2. Results of DSC runs for raw and torrefied PKS (20 K/min heating rate); (a) crucibles without a lid and (b) crucibles with a lid.

could be observed, related to decomposition reactions of primary pyrolysis products (secondary devolatilization).

As evident from the results shown in Figure 1b, the intensity of the first peak in the dTG curve reduced with increased torrefaction degree and almost disappeared, becoming a "shoulder", for torrefied PKS #3 (sample torrefied at 573 K). This indicated that the torrefaction process mainly affected hemicellulose, the most reactive component. This was in accordance with the results of Asadullah et al.,[20] who reported that the peak decreased in intensity for PKS samples prepared using a torrefaction temperature higher than 548 K and disappeared for the samples torrefied at 573 K. Qualitatively similar devolatilization behaviors were obtained for the different heating rates investigated in the present study (5−40 K/min).

The weight loss and weight loss rate curves recorded for torrefied PKS #2 using different heating rates are compared in Figure 1c and 1d, respectively. As expected, the higher the heating rate, the higher the devolatilization temperatures. This was observed for all the investigated samples.

Characteristic devolatilization parameters were evaluated from the results of TG runs. Table 3 summarizes the estimated parameters for the different samples and heating rates used, namely, the onset temperature, which was defined as the temperature at 5% of conversion, the temperature corresponding to the maximum weight loss rate, and the value of the maximum weight loss rate. The characteristic devolatilization parameters increased with the heating rate for all samples. The temperature at the maximum weight loss rate was almost the same for the parent and torrefied materials, while the onset temperature increased and the maximum weight loss rate decreased with increasing the torrefaction degree. The observed differences might be related to the different chemical compositions of the samples, namely, the increase in the onset temperature to a reduced hemicellulose content and the decrease in the maximum weight loss rate to a reduced cellulose content of the torrefied samples. This was confirmed by the results obtained for the chemical composition and is reported in Section 3.2.

Preliminary data with respect to the effect of the torrefaction pretreatment on the heat of pyrolysis of PKS were obtained from DSC analysis. A reliable assessment of the heat demand is important for the modeling of thermochemical processes. Furthermore, even if biomass pyrolysis is a globally endothermic process, any presence of exothermic reactions, which has been sometimes evidenced, can generate overheated zones in a reactor and even trigger a thermal runaway.[66] A wide variation of values is reported in the literature for the heat of pyrolysis of biomass feedstocks, ranging from exothermic to endothermic values.[46,66,67] Several factors have been invoked to explain the differences in the measured values of reaction enthalpy, such as secondary reactions between volatiles and char, which can be enhanced depending on the operating conditions (e.g., particle size), and catalytic effects due to the presence of inorganic species.[46,66,67]

Figure 2 shows the results of DSC runs carried out on the raw and torrefied PKS samples under different experimental conditions (in crucibles without a lid and with a pierced lid, Figure 2a,b, respectively). The absence of a lid promoted the evaporation of primary volatiles, thus reducing secondary interactions between the solid and volatiles. As evident from the comparison of Figures 2a and 1b, the DSC curves and the weight loss rate curves had similar shapes, at least for temperatures ranging from 500 to 670 K, and the peak temperatures matched, for the different samples. The pyrolysis process exhibited an endothermic behavior for all samples. An exothermic peak could be observed at higher temperatures (670−770 K). Anyway, global endothermic effects could be

https://doi.org/10.1021/acsomega.1c02141
ACS Omega 2021, 6, 20264−20278

Table 4. Results of the CHL Kinetic Model for the Investigated Biofuels (A in s^{-1})

CHL model	E [kJ/mol]	ln(A)		PKS	torrefied #1	torrefied #2	torrefied #3
hemicellulose	123.2	21.8	$x_{hemicellulose}$	0.356	0.286	0.284	0.216
cellulose	157.3	26.1	$x_{cellulose}$	0.415	0.405	0.404	0.360
lignin	44.0	1.5	x_{lignin}	0.229	0.309	0.312	0.424

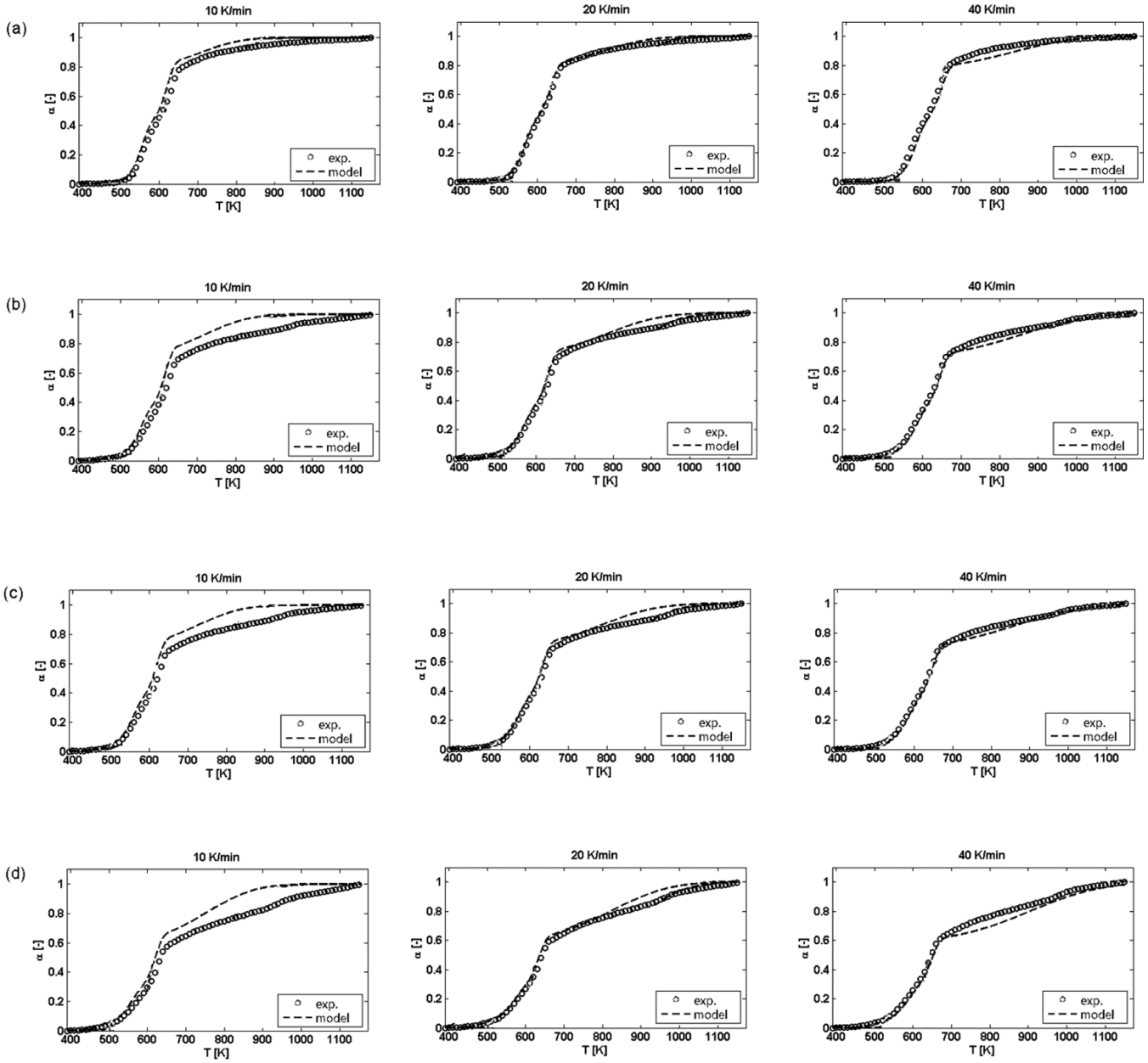

Figure 3. Comparison of experimental (symbols) and predicted (lines) conversion values by the CHL model at different heating rates for PKS (a), torrefied PKS #1 (b), torrefied PKS #2 (c), and torrefied PKS #3 (d).

evaluated for the pyrolysis of virgin and torrefied PKS by integrating the DSC curves over the entire temperature range. A significant decrease in the heat demand was found after the torrefaction pretreatment, the pyrolysis heat varying from 105 J/g for raw PKS to 9 J/g for torrefied PKS #3.

Completely different results were obtained in experimental runs carried out in crucibles with a pierced lid: in this case, the heat flow of the untreated and torrefied samples was completely in the exothermic region (Figure 2b). Previous studies suggest that the longer residence time of primary volatiles in contact with the solid enhances exothermic secondary reactions.[46,67] The results of the present study confirmed that secondary reactions can strongly affect the overall thermal effects of the process, which can shift from endothermic to exothermic. The exothermic effects in the pyrolysis of torrefied samples were less marked than those of virgin PKS (−144 J/g for raw PKS and −39 J/g for torrefied PKS #3).

These data showed that the torrefaction pretreatment had a significant influence on the heat of pyrolysis of biomass

https://doi.org/10.1021/acsomega.1c02141
ACS Omega 2021, 6, 20264−20278

Table 5. Kinetic Parameters Reported in the Literature for the Pyrolysis of Biomass Components

hemicellulose			cellulose			lignin			
n	E [kJ/mol]	A [s^{-1}]	n	E [kJ/mol]	A [s^{-1}]	n	E [kJ/mol]	A [s^{-1}]	ref
1	123.2	2.94×10^{9}	1	157.3	2.16×10^{11}	1	44.0	4.48	present study
			1	238	10^{18}				Antal and Varhegyi[60]
			1	238	10^{18}	1	34−65	$10^{0.3}$−10^{3}	Várhegyi et al.[48]
			1	201	1.14×10^{15}				Orfão et al.[49]
1	100	3.24×10^{6}	1	236	3.63×10^{17}	1	46	3.89	Grønli et al.[50]
1	194−200	4.7×10^{15}	1	243−251	1.0×10^{18}	1	37−62	0.7−69	Manyà et al.[51]
1	194−200	4.7×10^{15}	1	243−251	1.0×10^{18}	3	53.6−60.9	10^{2}	Manyà et al.[51]
1	183−197	4.5×10^{15}	1	240−248	10^{18}−10^{19}	3	58−94	10^{3}−10^{5}	Gómez et al.[52]
1	69.39	2.09×10^{3}	1	227.02	5.6×10^{16}	1−3	33.22		Yang et al.[53]
1	95−162	10^{6}−10^{12}	1	128−200	10^{8}−10^{15}	1	29−40	0.32−1.2	Hu et al.[54]
1.5−4	112−211	10^{7}−10^{17}	1.0−1.3	155−263	10^{10}−10^{20}	1.8−3.8	38−76	3−2.5×10^{4}	Hu et al.[54]
1	96−136	10^{7}−10^{10}	1	148−186	10^{10}−10^{13}	1	27−33	0.42−6.0	Li et al.[55]
1.1−2.1	98−141	10^{7}−10^{10}	1.1−1.3	175−202	10^{12}−10^{14}	1.3−3.7	30−52	0.7−2.2×10^{2}	Li et al.[55]
1	52−181	10−10^{15}	1	73−95	10^{3}−10^{7}	1	29−50	0.3−3	Damartzis et al.[56]
1	100.6	3.60×10^{6}	1	213.1	4.17×10^{15}	1	38.6	1.00	Broström et al.[57]
1	105.19	2.03×10^{7}	1	193.64	1.25×10^{14}	1	38.43	1.78	Bach et al.[41]

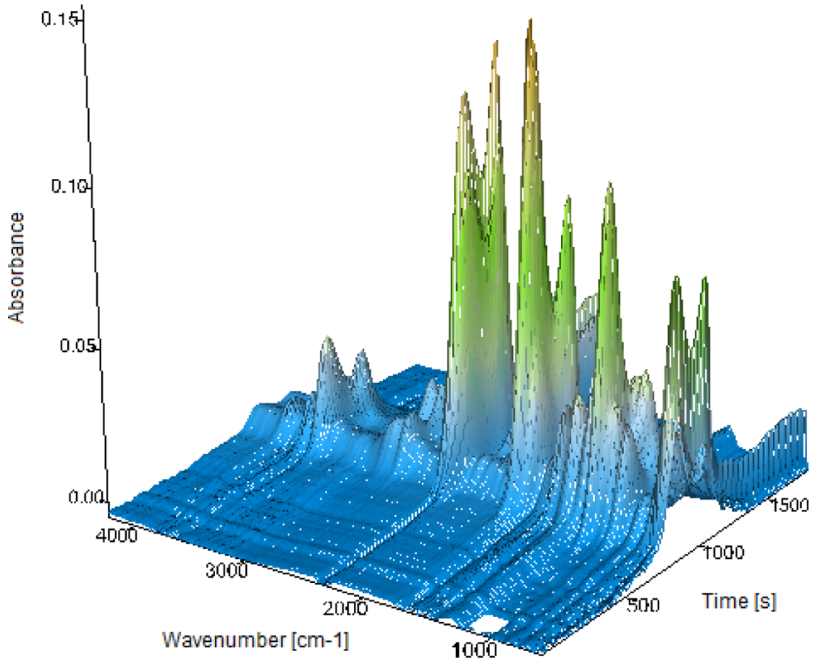

Figure 4. 3D FTIR analysis of evolved gases in a TG-FTIR devolatilization run performed on PKS (20 K/min heating rate).

samples: increasing the torrefaction severity led to a reduction of either endothermic or exothermic effects. This was probably due to the changes in the chemical structure of biomass after torrefaction. The reduced content of low-temperature degrading components (hemicellulose) in the torrefied samples probably caused a reduction in the endothermic effects observed in the absence of a lid. At the same time, the reduced release of VM from torrefied samples led to a reduction of the concentration of vapor-phase species and thus to a reduction of the exothermic secondary reactions between volatiles and the solid.

3.2. Devolatilization Kinetics. The devolatilization model described in Section 2.3, named the CHL model and based on three parallel first-order reactions corresponding to biomass components (cellulose, hemicellulose, and lignin), was applied for the analysis of the data acquired in the TG runs performed on raw and torrefied PKS samples.

The application of the model yielded the values of the kinetic parameters (activation energy and pre-exponential factor) for the components, which were the same for all materials, and the chemical composition for each biofuel. Indeed, previous studies[41,57] on the pyrolysis kinetics of torrefied spruce wood had revealed that the torrefaction pretreatment did not affect the reactivity (i.e., activation energy and pre-exponential factor) of the wood components, hemicellulose, cellulose, and lignin, but only their relative amounts.

The results of the CHL model are reported in Table 4, while Figure 3 compares the predicted conversion values with the experimental ones for raw and torrefied PKS at different heating rates. The good agreement between experimental and simulated curves can be clearly observed in Figure 3.

Compared to hemicellulose and cellulose, lignin had a low activation energy (44 kJ/mol) and its pre-exponential factor

https://doi.org/10.1021/acsomega.1c02141
ACS Omega 2021, 6, 20264−20278

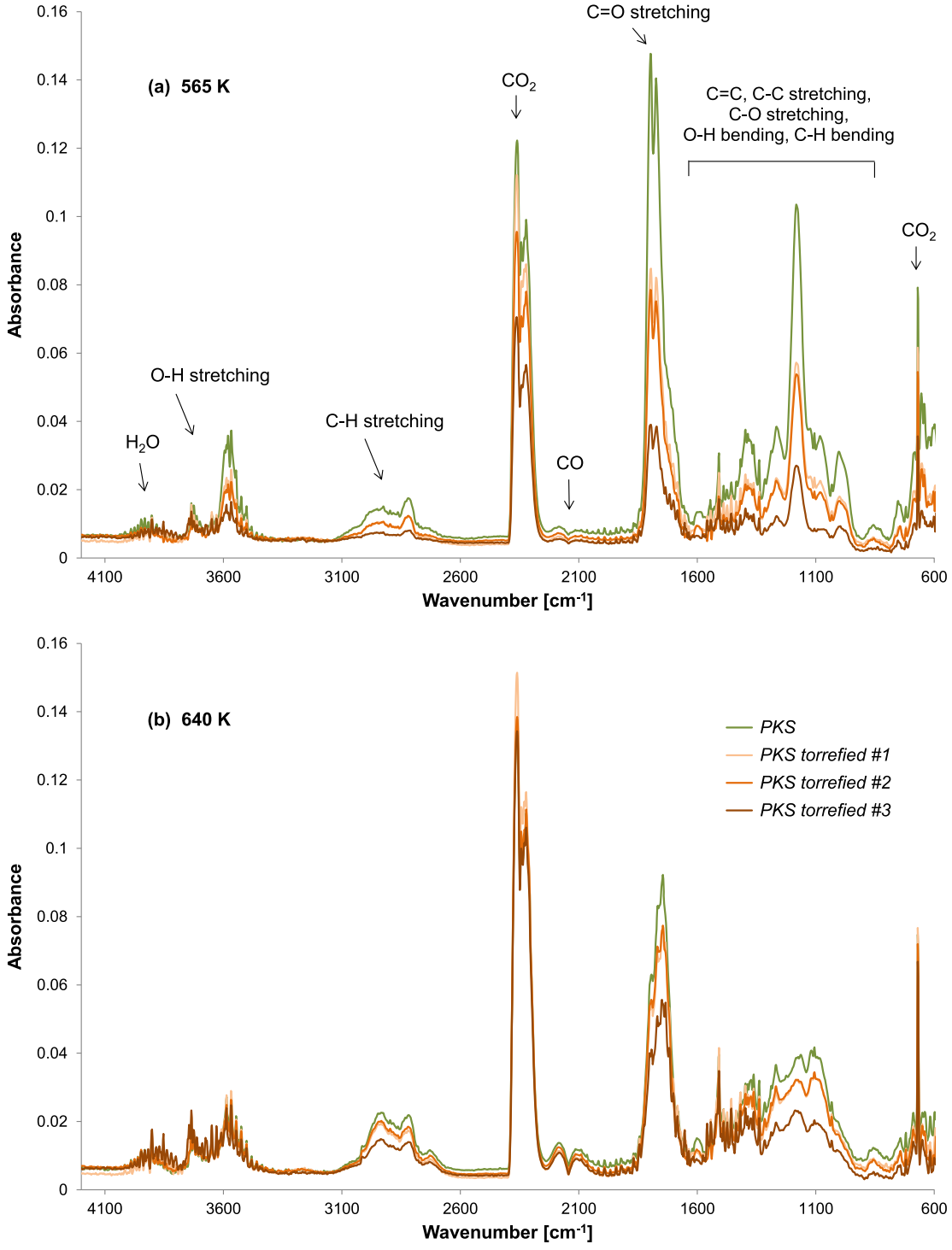

Figure 5. FTIR spectra of evolved gases in TG-FTIR devolatilization runs performed on raw and torrefied PKS (20 K/min heating rate): (a) FTIR spectra of the volatiles evolved at 565 K (temperature corresponding to the first devolatilization peak) and (b) FTIR spectra of the volatiles evolved at 640 K (temperature corresponding to the main devolatilization peak).

was also low. Activation energies of 123 and 157 kJ/mol were evaluated for hemicellulose and cellulose, respectively. The values obtained for the kinetic parameters were consistent with those reported in the literature.[68] Table 5 summarizes the values of the kinetic parameters reported in literature studies for the pyrolysis of biomass components.[41,48−57,60] Previous publications indicated activation energies in the range of 100−250 kJ/mol for cellulose. A lower activation energy value than that for cellulose was usually reported for the hemicellulose component, but it was still high (50−200 kJ/mol). The value for the lignin component was generally quite low (30−70 kJ/mol).

As for the chemical composition, the results obtained highlighted that the torrefaction process led to a significant reduction in the hemicellulose content (from 35.0% for raw PKS to 16.4% for torrefied PKS #3), a slight reduction in the cellulose content (from 41.5% for PKS to 36.0% for torrefied PKS #3), and a corresponding increase in the lignin fraction

https://doi.org/10.1021/acsomega.1c02141
ACS Omega 2021, 6, 20264−20278

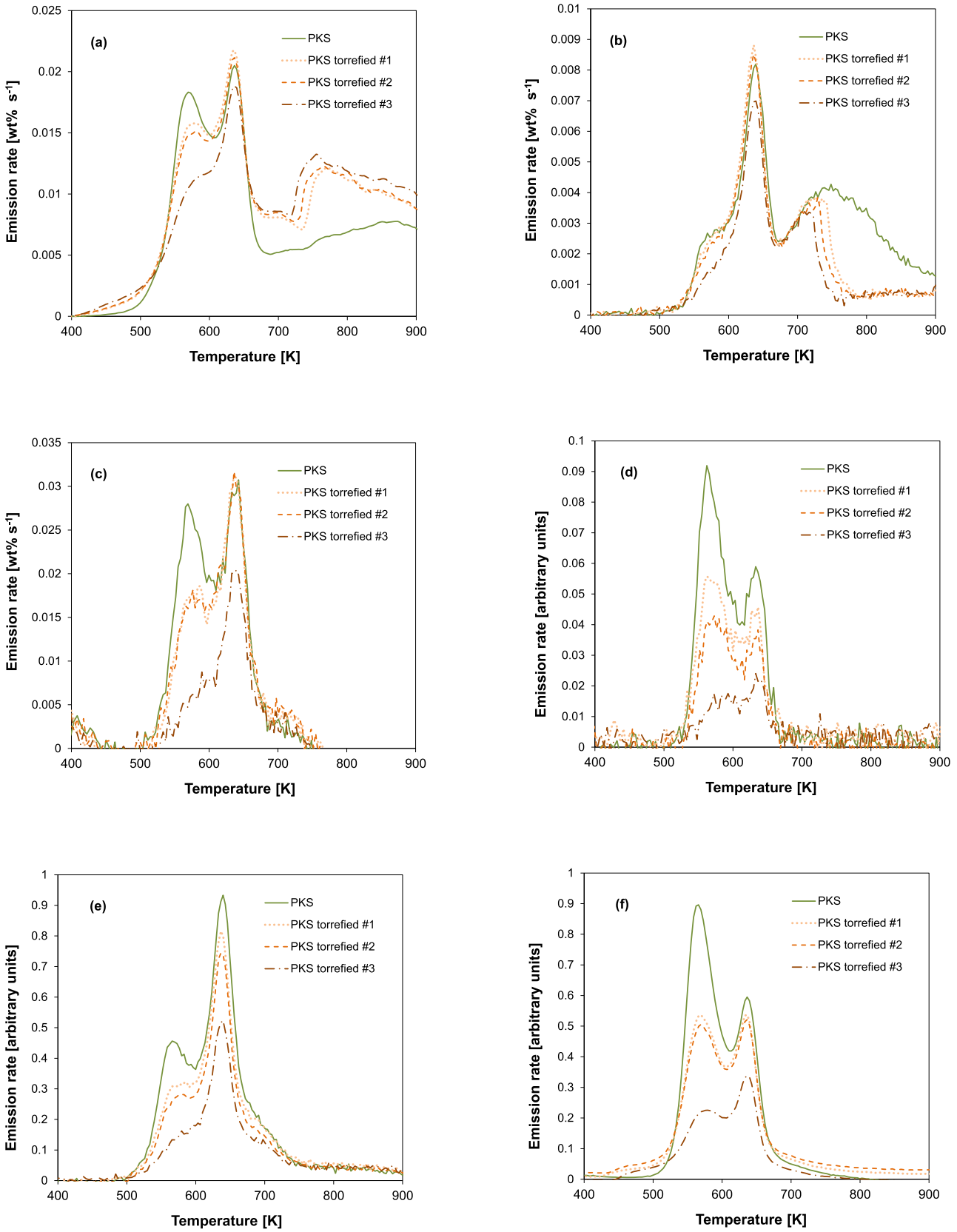

Figure 6. Results of evolved gas analysis for TG-FTIR devolatilization runs performed on PKS with different torrefaction degrees (20 K/min heating rate): emission profiles of carbon dioxide (a), carbon monoxide (b), water (c), formic acid (d), hydrocarbon compounds (e), and carbonyl compounds (f).

(from 22.9% for PKS to 42.4% for torrefied PKS #3). These results reflected the experimental evidence based on TG data,

https://doi.org/10.1021/acsomega.1c02141
ACS Omega 2021, 6, 20264−20278

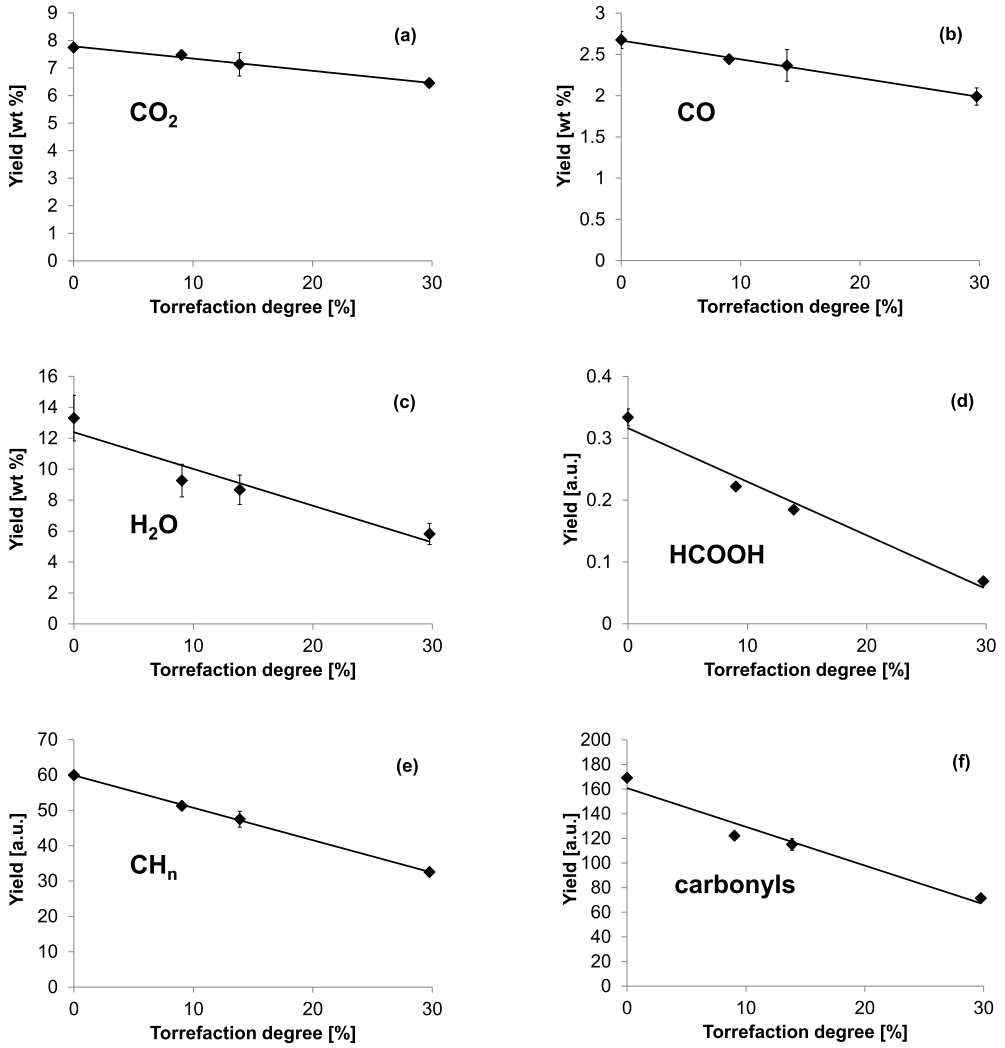

Figure 7. Results of the quantitative analysis of evolved gases in TG-FTIR devolatilization runs: correlation between the torrefaction degree of PKS samples and quantities of evolved carbon dioxide (a), carbon monoxide (b), water (c), formic acid (d), hydrocarbon compounds (e), and carbonyl compounds (f).

indicating a reduction of the devolatilization peak ascribed to the hemicellulose component with increasing the torrefaction temperature (see Figure 1 and Section 3.1).

The present results are in accordance with previous studies, which pointed out that the torrefaction process is characterized by a reduction of hemicellulose content, even for torrefaction temperatures as low as 503 K, whereas cellulose is affected only when severe torrefaction is applied (temperatures around 563 K), and a negligible impact on lignin is detected.[69,70] An increasing contribution of the lignin component in torrefied fuels is therefore expected with the increase in the severity of torrefaction conditions. This was observed as well by Broström et al.[57] for torrefied spruce wood.

3.3. Devolatilization Products. The characterization of volatile products evolved during biofuel devolatilization was performed by TG-FTIR analysis.

Figure 4 shows the typical results of the online FTIR analysis of the volatiles evolved during a run performed on PKS. Representative infrared spectra of the volatiles generated in the TG-FTIR pyrolysis runs carried out on raw and torrefied PKS samples are shown in Figure 5. Figure 5a,b reports the FTIR spectra recorded in correspondence to the peaks in the weight loss rate curves, that is, at 565 K (first devolatilization peak) and 640 K (main devolatilization peak), respectively. As expected for the pyrolysis of biomass substrates, a complex mixture of products including gases (e.g., carbon dioxide and carbon monoxide), water, and higher-molecular-weight organic compounds evolved. The characteristic absorption bands of the identified components and functional groups are indicated in Figure 5.

Following the procedure described in Section 2.4, the evolution profiles of the different volatile species released as a function of sample temperature were determined. Figure 6 compares the emission profiles of the main compounds and classes of compounds obtained in experimental runs carried out with PKS and torrefied PKS samples, namely, carbon dioxide (Figure 6a), carbon monoxide (Figure 6b), water (Figure 6c), formic acid (Figure 6d), hydrocarbon compounds (Figure 6e), and carbonyl compounds (Figure 6f). While quantitative data were achieved for carbon dioxide, carbon monoxide, and water, the data related to organic compounds were normalized by the initial dry sample mass and reported in arbitrary units in Figures 6 and 7. Anyway, the present approach allowed us to compare the emission rate and the amount evolved of a specific volatile species released by different samples.

https://doi.org/10.1021/acsomega.1c02141
ACS Omega 2021, 6, 20264−20278

Table 6. Correlation Parameters Between the Yield of Specific Devolatilization Products and the Torrefaction Degree for PKS Samples

product	CO_2	CO	water	formic acid	hydrocarbon compounds	carbonyl compounds
coefficient of determination r^2	0.9884	0.9974	0.9227	0.9776	0.9994	0.9590
yield percentage variation (% variation/% torr degree)	−0.571	−0.854	−1.92	−2.75	−1.53	−1.95

A strong correspondence was observed between volatile emission profiles and the weight loss behavior, as evident from the comparison of Figures 6 and 1b. The different species were released in the same temperature range of the primary devolatilization, with a composite shape of the emission profile which corresponded to the composite shape of the weight loss rate curve, the maxima of IR profiles corresponding to the maximum rate of weight loss. The release of carbon monoxide and carbon dioxide was detected as well during the devolatilization tail (or secondary devolatilization). The emission patterns can be related to the decomposition of the different biomass chemical components, that is, cellulose, hemicellulose, and lignin. Indeed, a large number of studies have been devoted to the investigation of the pyrolysis products and mechanism of lignocellulosic biomass constituents.[71,72]

Cellulose is a linear homopolysaccharide composed of glucose units linked by β-1,4-glycosidic bonds, with a degree of polymerization which may be as high as 15,000. Dehydration reactions and cleavage of glycosidic bonds with consequent cellulose depolymerization are the main reactions occurring in the initial stage of pyrolysis (i.e., at temperatures lower than 573 K).[71,72] For temperatures higher than 573 K, the high depolymerization rate of cellulose leads to the formation of relevant yields of anhydro-sugars and furans, such as 5-hydroxymethylfurfural, 5-methylfurfural, furfural, and furfuryl alcohol.[71,72] Further dehydration and fragmentation reactions are responsible for the significant production of water, CO, CO_2, and small-chain carbonyl compounds (i.e., acetaldehyde, hydroxyacetaldehyde, and hydroxyacetone).[71,72]

On the other hand, hemicellulose is composed of short-chain heteropolysaccharides, whose composition varies depending on plant species; in addition, the hemicellulose structure includes some uronic acids and acetyl groups. The release of water, due to dehydration reactions within the polysaccharides, and the breaking of less stable linkages become significant at temperatures higher than 473 K.[71,72] The fragmentation of the carboxylic acid function of uronic acids and acetyl groups mainly contributes to the formation of carbon dioxide, formic acid, and acetic acid.[71,72] With a temperature increase to around 523 K, the glycosidic linkages between monomer units become very unstable and a rapid depolymerization occurs, leading to the formation of different anhydro-sugars and furans.[71,72] The depolymerization of the hemicellulose generates unstable intermediates which undergo dehydration, fragmentation, and secondary reactions, yielding significant quantities of water, CO, CO_2 hydroxyacetaldehyde, hydroxyacetone, 1-hydroxy-2-butanone, acetic acid, and cyclopentenones.[71,72]

In contrast to the saccharide structure of cellulose and hemicellulose, lignin has an aromatic matrix. The thermal degradation of lignin occurs over a large temperature range, due to the successive cleavage of different linkages (e.g., ether bonds and carbon−carbon bonds) as the reaction temperature increases.[71,72] The breaking of bonds between the monomer units causes the formation of relevant yields of phenolic compounds.[71,72] The presence of oxygenated groups in the lignin structure, such as carboxyl and carbonyl groups, leads to the release of carbon dioxide, carbon monoxide, and formaldehyde, while methane and methanol are mainly evolved from methoxy groups.[71,72]

The results reported in Figure 6 evidenced that torrefaction and the increase in the severity of torrefaction conditions entailed a decrease in the evolution of the volatile products evolved, especially in correspondence of the shoulder associated with hemicellulose decomposition. This trend was particularly evident for water, formic acid, hydrocarbon, and carbonyl compounds. Qualitatively similar results were reported by Ma et al.[73] in their investigation of the pyrolysis characteristics of PKS by TG-FTIR analysis.

The yields of the main volatile products formed in the devolatilization process were assessed. Figure 7 summarizes the results of the quantitative analysis, specifically the amounts of main evolved species with respect to dry fuel weight. The values were calculated in the temperature range corresponding to the primary devolatilization (i.e., up to a maximum temperature of 723 K).

Relevant quantities of pyrolytic water were generated in the devolatilization process, about 13.3 (±1.5) weight % with respect to dry fuel weight in the case of raw PKS. This value was in line with those reported in the literature: Neves et al.[74] indicated a yield of pyrolytic water within 5−20%, based on data collected from several literature studies, involving various biomass feedstocks, reactors, and experimental conditions. Among permanent gases, significant quantities of carbon dioxide and carbon monoxide were formed, 7.75 (±0.16) and 2.68 (±0.10) weight % with respect to dry sample weight, respectively, in the pyrolysis of raw PKS. These data were in agreement with the findings of Neves et al.,[74] who reported that CO_2 and CO were the main gas species arising from the primary decomposition of biomass, with approximate yields of 5−16 mass % of dry ash-free fuel for CO_2 and 2−8 mass % of dry ash-free fuel for CO and a CO_2/CO ratio of ≈2−3.5, at temperatures of 723−823 K, along with lower amounts of methane and other light hydrocarbons (roughly 1%).

It should be pointed out that hydrogen, a further gaseous pyrolytic product, is infrared inactive, so it could not be detected. Anyway, literature data indicate that hydrogen production during primary pyrolysis is very limited (<0.2 wt % below 723 K).[74,75] Several studies suggest that hydrogen production is related to the charring process and becomes significant at temperatures higher than 773 K: for temperatures higher than 773 K, considerable amounts of H_2 and CO are released from char, which evolves toward a more condensed polycyclic aromatic structure.[71,72]

Lower volatile yields were measured for torrefied PKS samples. Figure 7 shows the yields of the different volatile pyrolysis products as a function of the torrefaction degree. Specific linear correlations between volatile yields and the torrefaction degree for PKS samples could be observed. The higher the torrefaction degree, the lower the specific volatile production. The values of the coefficient of determination r^2

https://doi.org/10.1021/acsomega.1c02141
ACS Omega 2021, 6, 20264−20278

and the percentage variation of the yield of a specific devolatilization product with respect to the torrefaction degree, calculated on the best linear fitting, are reported in Table 6.

The results in Figure 7 and Table 6 indicated a high correlation between the production of the identified pyrolysis products and the degree of torrefaction ($r^2 > 0.9$); particularly high values of the coefficient of determination were obtained for carbon dioxide (r^2 0.9884), carbon monoxide (r^2 0.9974), and hydrocarbons (r^2 0.9994). The values of the yield percentage variation with respect to the torrefaction degree suggested that the reduction on the volatiles production caused by the torrefaction process was significantly higher for water and for organic compounds (hydrocarbons and carbonyls) than for carbon oxides. A volatile fraction with reduced contents of water and low-molecular-weight carbonyl and/or carboxylic compounds may thus be expected from the pyrolysis of torrefied materials. As a matter of fact, dehydration reactions of hydroxyl groups and fragmentation reactions of the carboxylic acid functions in branches were reported as the main reactions occurring during torrefaction.[72] The highest reduction in volatile production was observed for formic acid, which is a typical pyrolysis product of hemicellulose.[71,72] This was a further confirmation that the specific features of volatile emission were related to the decomposition of the different biomass chemical components and that the torrefaction process mainly affected the hemicellulose content.[69,70,72]

4. CONCLUSIONS

The effect of torrefaction on biomass devolatilization characteristics, including kinetics, heat demand, speciation, and quantities of volatile products evolved, was investigated in order to provide fundamental information for the design and operation of thermochemical conversion units using torrefied feedstocks.

The application of the CHL devolatilization model based on three parallel first-order reactions corresponding to biomass components was able to satisfactorily reproduce the thermal decomposition behavior of the investigated biofuels. Activation energies of 123, 157, and 44 kJ/mol were evaluated for hemicellulose, cellulose, and lignin, respectively. As for the chemical composition, torrefaction led to a significant reduction in the hemicellulose content (from 35.0% for raw PKS to 16.4% for torrefied PKS #3), a slight reduction in the cellulose content (from 41.5% for PKS to 36.0% for torrefied PKS #3), and a corresponding increase in the lignin fraction (from 22.9% for PKS to 42.4% for torrefied PKS #3). Increasing the severity of the torrefaction pretreatment led to a reduction of the thermal effects of the pyrolysis process, the pyrolysis heat decreasing from 105 J/g for PKS to 9 J/g for torrefied PKS #3.

The emission characteristics and the yields of the main volatile products formed during primary devolatilization were assessed. The results obtained indicated that the reduction in the volatile production caused by the torrefaction pretreatment was significantly higher for water and for organic compounds than for carbon monoxide and carbon dioxide. A volatile fraction with reduced contents of water and low-molecular-weight carbonyl and/or carboxylic compounds may thus be expected from the pyrolysis of torrefied materials.

AUTHOR INFORMATION

Corresponding Author

Federica Barontini − *Dipartimento di Ingegneria Civile e Industriale, Università di Pisa, Pisa, Largo Lucio Lazzarino 56122, Italy*; orcid.org/0000-0002-6293-8358; Email: federica.barontini@unipi.it

Authors

Enrico Biagini − *Dipartimento di Ingegneria Civile e Industriale, Università di Pisa, Pisa, Largo Lucio Lazzarino 56122, Italy*

Leonardo Tognotti − *Dipartimento di Ingegneria Civile e Industriale, Università di Pisa, Pisa, Largo Lucio Lazzarino 56122, Italy*

Complete contact information is available at: https://pubs.acs.org/10.1021/acsomega.1c02141

Notes

The authors declare no competing financial interest.

NOMENCLATURE

A, pre-exponential factor
$\mathcal{A}$, absorbance
b, heating rate
c, concentration
D, integral of I with respect to time
E, activation energy
I, integrated absorbance
K, experimental correlation factor relating I to concentration
K', experimental correlation factor relating D to m
l, optical path length
m, total amount of the compound evolved
n, order of reaction
R, universal gas constant
r^2, coefficient of determination
T, absolute temperature
t, time
w, weight mass of the solid phase
wt, weight
x, mass fraction of chemical components
α, devolatilization conversion
ε, molar extinction coefficient
$\tilde{\nu}$, wavenumber

SUBSCRIPTS AND SUPERSCRIPTS

0	initial value
∞	final value
i	index for biomass
j	index for the chemical component
max	maximum value
torr	torrefied

ABBREVIATIONS

ar	as-received
CHL	cellulose hemicellulose lignin (kinetic model)
daf	dry and ash-free
DSC	differential scanning calorimetry
dTG	derivative thermogravimetric
FC	fixed carbon
FTIR	Fourier transformed infrared spectroscopy
HHV	higher heating value

https://doi.org/10.1021/acsomega.1c02141
ACS Omega 2021, 6, 20264−20278

LHV	lower heating value
PKS	palm kernel shell
TG	thermogravimetric
torrefied PKS #1	torrefied palm kernel shell (473 K, 30 min)
torrefied PKS #2	torrefied palm kernel shell (523 K, 30 min)
torrefied PKS #3	torrefied palm kernel shell (573 K, 30 min)
VM	volatile matter

REFERENCES

(1) van der Stelt, M. J. C.; Gerhauser, H.; Kiel, J. H. A.; Ptasinski, K. J. Biomass upgrading by torrefaction for the production of biofuels: a review. *Biomass Bioenergy* **2011**, *35*, 3748−3762.

(2) Chen, W.-H.; Peng, J.; Bi, X. T. A state-of-the-art review of biomass torrefaction, densification and applications. *Renewable Sustainable Energy Rev.* **2015**, *44*, 847−866.

(3) Barskov, S.; Zappi, M.; Buchireddy, P.; Dufreche, S.; Guillory, J.; Gang, D.; Hernandez, R.; Bajpai, R.; Baudier, J.; Cooper, R.; Sharp, R. Torrefaction of biomass: A review of production methods for biocoal from cultured and waste lignocellulosic feedstocks. *Renewable Energy* **2019**, *142*, 624−642.

(4) Niu, Y.; Lv, Y.; Lei, Y.; Liu, S.; Liang, Y.; Wang, D.; Hui, S. e. Biomass torrefaction: properties, applications, challenges, and economy. *Renewable Sustainable Energy Rev.* **2019**, *115*, 109395.

(5) Cahyanti, M. N.; Doddapaneni, T. R. K. C.; Kikas, T. Biomass torrefaction: An overview on process parameters, economic and environmental aspects and recent advancements. *Bioresour. Technol.* **2020**, *301*, 122737.

(6) Chiou, B.-S.; Valenzuela-Medina, D.; Bilbao-Sainz, C.; Klamczynski, A. P.; Avena-Bustillos, R. J.; Milczarek, R. R.; Du, W.-X.; Glenn, G. M.; Orts, W. J. Torrefaction of almond shells: Effects of torrefaction conditions on properties of solid and condensate products. *Ind. Crops Prod.* **2016**, *86*, 40−48.

(7) Gogoi, D.; Bordoloi, N.; Goswami, R.; Narzari, R.; Saikia, R.; Sut, D.; Gogoi, L.; Kataki, R. Effect of torrefaction on yield and quality of pyrolytic products of arecanut husk: An agro-processing wastes. *Bioresour. Technol.* **2017**, *242*, 36−44.

(8) Chen, W.-H.; Lu, K.-M.; Tsai, C.-M. An experimental analysis on property and structure variations of agricultural wastes undergoing torrefaction. *Appl. Energy* **2012**, *100*, 318−325.

(9) Tian, X.; Dai, L.; Wang, Y.; Zeng, Z.; Zhang, S.; Jiang, L.; Yang, X.; Yue, L.; Liu, Y.; Ruan, R. Influence of torrefaction pretreatment on corncobs: A study on fundamental characteristics, thermal behavior, and kinetic. *Bioresour. Technol.* **2020**, *297*, 122490.

(10) Nam, H.; Capareda, S. Experimental investigation of torrefaction of two agricultural wastes of different composition using RSM (response surface methodology). *Energy* **2015**, *91*, 507−516.

(11) Deng, J.; Wang, G.-J.; Kuang, J.-H.; Zhang, Y.-L.; Luo, Y.-H. Pretreatment of agricultural residues for co-gasification via torrefaction. *J. Anal. Appl. Pyrolysis* **2009**, *86*, 331−337.

(12) Cai, W.; Fivga, A.; Kaario, O.; Liu, R. Effects of Torrefaction on the Physicochemical Characteristics of Sawdust and Rice Husk and Their Pyrolysis Behavior by Thermogravimetric Analysis and Pyrolysis-Gas Chromatography/Mass Spectrometry. *Energy Fuels* **2017**, *31*, 1544−1554.

(13) Chen, D.; Gao, A.; Ma, Z.; Fei, D.; Chang, Y.; Shen, C. In-depth study of rice husk torrefaction: Characterization of solid, liquid and gaseous products, oxygen migration and energy yield. *Bioresour. Technol.* **2018**, *253*, 148−153.

(14) Bridgeman, T. G.; Jones, J. M.; Shield, I.; Williams, P. T. Torrefaction of reed canary grass, wheat straw and willow to enhance solid fuel qualities and combustion properties. *Fuel* **2008**, *87*, 844−856.

(15) Jian, J.; Lu, Z.; Yao, S.; Li, X.; Song, W. Comparative Study on Pyrolysis of Wet and Dry Torrefied Beech Wood and Wheat Straw. *Energy Fuels* **2019**, *33*, 3267−3274.

(16) Valix, M.; Katyal, S.; Cheung, W. H. Combustion of thermochemically torrefied sugar cane bagasse. *Bioresour. Technol.* **2017**, *223*, 202−209.

(17) Benavente, V.; Fullana, A. Torrefaction of olive mill waste. *Biomass Bioenergy* **2015**, *73*, 186−194.

(18) Martín-Lara, M. A.; Ronda, A.; Zamora, M. C.; Calero, M. Torrefaction of olive tree pruning: Effect of operating conditions on solid product properties. *Fuel* **2017**, *202*, 109−117.

(19) Sabil, K. M.; Aziz, M. A.; Lal, B.; Uemura, Y. Effects of torrefaction on the physiochemical properties of oil palm empty fruit bunches, mesocarp fiber and kernel shell. *Biomass Bioenergy* **2013**, *56*, 351−360.

(20) Asadullah, M.; Adi, A. M.; Suhada, N.; Malek, N. H.; Saringat, M. I.; Azdarpour, A. Optimization of palm kernel shell torrefaction to produce energy densified bio-coal. *Energy Convers. Manage.* **2014**, *88*, 1086−1093.

(21) Uemura, Y.; Saadon, S.; Osman, N.; Mansor, N.; Tanoue, K.-I. Torrefaction of oil palm kernel shell in the presence of oxygen and carbon dioxide. *Fuel* **2015**, *144*, 171−179.

(22) Chen, W.-H.; Zhuang, Y.-Q.; Liu, S.-H.; Juang, T.-T.; Tsai, C.-M. Product characteristics from the torrefaction of oil palm fiber pellets in inert and oxidative atmospheres. *Bioresour. Technol.* **2016**, *199*, 367−374.

(23) Poudel, J.; Ohm, T.-I.; Gu, J. H.; Shin, M. C.; Oh, S. C. Comparative study of torrefaction of empty fruit bunches and palm kernel shell. *J. Mater. Cycles Waste Manage.* **2017**, *19*, 917−927.

(24) Sukiran, M. A.; Abnisa, F.; Wan Daud, W. M. A.; Abu Bakar, N.; Loh, S. K. A review of torrefaction of oil palm solid wastes for biofuel production. *Energy Convers. Manage.* **2017**, *149*, 101−120.

(25) Talero, G.; Rincón, S.; Gómez, A. Biomass torrefaction in a standard retort: A study on oil palm solid residues. *Fuel* **2019**, *244*, 366−378.

(26) Ahmad, R.; Mohd Ishak, M. A.; Kasim, N. N.; Ismail, K. Properties and thermal analysis of upgraded palm kernel shell and Mukah Balingian coal. *Energy* **2019**, *167*, 538−547.

(27) Junga, R.; Pospolita, J.; Niemiec, P. Combustion and grindability characteristics of palm kernel shells torrefied in a pilot-scale installation. *Renewable Energy* **2020**, *147*, 1239−1250.

(28) Sukiran, M. A.; Abnisa, F.; Syafiie, S.; Wan Daud, W. M. A.; Nasrin, A. B.; Abdul Aziz, A.; Loh, S. K. Experimental and modelling study of the torrefaction of empty fruit bunches as a potential fuel for palm oil mill boilers. *Biomass Bioenergy* **2020**, *136*, 105530.

(29) Proskurina, S.; Heinimö, J.; Schipfer, F.; Vakkilainen, E. Biomass for industrial applications: The role of torrefaction. *Renewable Energy* **2017**, *111*, 265−274.

(30) Couhert, C.; Salvador, S.; Commandré, J.-M. Impact of torrefaction on syngas production from wood. *Fuel* **2009**, *88*, 2286−2290.

(31) Cerone, N.; Zimbardi, F.; Villone, A.; Strjiugas, N.; Kiyikci, E. G. Gasification of Wood and Torrefied Wood with Air, Oxygen, and Steam in a Fixed-Bed Pilot Plant. *Energy Fuels* **2016**, *30*, 4034−4043.

(32) Di Marcello, M.; Tsalidis, G. A.; Spinelli, G.; de Jong, W.; Kiel, J. H. A. Pilot scale steam-oxygen CFB gasification of commercial torrefied wood pellets. The effect of torrefaction on the gasification performance. *Biomass Bioenergy* **2017**, *105*, 411−420.

(33) Pinto, F.; Gominho, J.; André, R. N.; Gonçalves, D.; Miranda, M.; Varela, F.; Neves, D.; Santos, J.; Lourenço, A.; Pereira, H. Effect of Rice Husk Torrefaction on Syngas Production and Quality. *Energy Fuels* **2017**, *31*, 5183−5192.

(34) Pinto, F.; Gominho, J.; André, R. N.; Gonçalves, D.; Miranda, M.; Varela, F.; Neves, D.; Santos, J.; Lourenço, A.; Pereira, H. Improvement of gasification performance of Eucalyptus globulus stumps with torrefaction and densification pre-treatments. *Fuel* **2017**, *206*, 289−299.

(35) Woytiuk, K.; Campbell, W.; Gerspacher, R.; Evitts, R. W.; Phoenix, A. The effect of torrefaction on syngas quality metrics from fluidized bed gasification of SRC willow. *Renewable Energy* **2017**, *101*, 409−416.

https://doi.org/10.1021/acsomega.1c02141
ACS Omega 2021, 6, 20264−20278

(36) Al-Farraji, A.; Marsh, R.; Steer, J.; Valera-Medina, A. Kinetics and Performance of Raw and Torrefied Biomass in a Continuous Bubbling Fluidized Bed Gasifier. *Waste Biomass Valorization* **2019**, *10*, 1365−1381.
(37) Louwes, A. C.; Basile, L.; Yukananto, R.; Bhagwandas, J. C.; Bramer, E. A.; Brem, G. Torrefied biomass as feed for fast pyrolysis: An experimental study and chain analysis. *Biomass Bioenergy* **2017**, *105*, 116−126.
(38) Mi, B.; Liu, Z.; Hu, W.; Wei, P.; Jiang, Z.; Fei, B. Investigating pyrolysis and combustion characteristics of torrefied bamboo, torrefied wood and their blends. *Bioresour. Technol.* **2016**, *209*, 50−55.
(39) Cao, L.; Yuan, X.; Jiang, L.; Li, C.; Xiao, Z.; Huang, Z.; Chen, X.; Zeng, G.; Li, H. Thermogravimetric characteristics and kinetics analysis of oil cake and torrefied biomass blends. *Fuel* **2016**, *175*, 129−136.
(40) Doddapaneni, T. R. K. C.; Konttinen, J.; Hukka, T. I.; Moilanen, A. Influence of torrefaction pretreatment on the pyrolysis of Eucalyptus clone: A study on kinetics, reaction mechanism and heat flow. *Ind. Crops Prod.* **2016**, *92*, 244−254.
(41) Bach, Q.-V.; Trinh, T. N.; Tran, K.-Q.; Thi, N. B. D. Pyrolysis characteristics and kinetics of biomass torrefied in various atmospheres. *Energy Convers. Manage.* **2017**, *141*, 72−78.
(42) Singh, S.; Prasad Chakraborty, J.; Kumar Mondal, M. Intrinsic kinetics, thermodynamic parameters and reaction mechanism of non-isothermal degradation of torrefied Acacia nilotica using isoconversional methods. *Fuel* **2020**, *259*, 116263.
(43) Gan, M. J.; Lim, W. S.; Ng, H. X.; Ong, M. H.; Gan, S.; Lee, L. Y.; Thangalazhy-Gopakumar, S. Enhancement of Palm Kernel Shell Fuel Properties via Wet Torrefaction: Response Surface, Optimization, and Combustion Studies. *Energy Fuels* **2019**, *33*, 11009−11020.
(44) Ahmad, F. B.; Zhang, Z.; Doherty, W. O. S.; O'Hara, I. M. The outlook of the production of advanced fuels and chemicals from integrated oil palm biomass biorefinery. *Renewable Sustainable Energy Rev.* **2019**, *109*, 386−411.
(45) Li, J.; Bonvicini, G.; Tognotti, L.; Yang, W.; Blasiak, W. High-temperature rapid devolatilization of biomasses with varying degrees of torrefaction. *Fuel* **2014**, *122*, 261−269.
(46) Rath, J.; Wolfinger, M. G.; Steiner, G.; Krammer, G.; Barontini, F.; Cozzani, V. Heat of Wood Pyrolysis. *Fuel* **2003**, *82*, 81−91.
(47) White, J. E.; Catallo, W. J.; Legendre, B. L. Biomass pyrolysis kinetics: A Comparative critical review with relevant agricultural residue case studies. *J. Anal. Appl. Pyrolysis* **2011**, *91*, 1−33.
(48) Várhegyi, G.; Antal, M. J., Jr.; Jakab, E.; Szabó, P. Kinetic modeling of biomass pyrolysis. *J. Anal. Appl. Pyrolysis* **1997**, *42*, 73−87.
(49) Orfão, J. J. M.; Antunes, F. J. A.; Figueiredo, J. L. Pyrolysis kinetics of lignocellulosic materials − three independent reactions model. *Fuel* **1999**, *78*, 349−358.
(50) Grønli, M. G.; Varhegyi, G.; Di Blasi, C. Thermogravimetric Analysis and Devolatilization Kinetics of Wood. *Ind. Eng. Chem. Res.* **2002**, *41*, 4201−4208.
(51) Manyà, J. J.; Velo, E.; Puigjaner, L. Kinetics of Biomass Pyrolysis: a Reformulated Three-Parallel-Reactions Model. *Ind. Eng. Chem. Res.* **2003**, *42*, 434−441.
(52) Gómez, C. J.; Manyà, J. J.; Velo, E.; Puigjaner, L. Further Applications of a Revisited Summative Model for Kinetics of Biomass Pyrolysis. *Ind. Eng. Chem. Res.* **2004**, *43*, 901−906.
(53) Yang, H.; Yan, R.; Chin, T.; Liang, D. T.; Chen, H.; Zheng, C. Thermogravimetric Analysis − Fourier Transform Infrared Analysis of Palm Oil Waste Pyrolysis. *Energy Fuels* **2004**, *18*, 1814−1821.
(54) Hu, S.; Jess, A.; Xu, M. Kinetic study of Chinese biomass slow pyrolysis: Comparison of different kinetic models. *Fuel* **2007**, *86*, 2778−2788.
(55) Li, Z.; Zhao, W.; Meng, B.; Liu, C.; Zhu, Q.; Zhao, G. Kinetic study of corn straw pyrolysis: Comparison of two different three-pseudocomponent models. *Bioresour. Technol.* **2008**, *99*, 7616−7622.
(56) Damartzis, T.; Vamvuka, D.; Sfakiotakis, S.; Zabaniotou, A. Thermal degradation studies and kinetic modeling of cardoon (Cynara cardunculus) pyrolysis using thermogravimetric analysis (TGA). *Bioresour. Technol.* **2011**, *102*, 6230−6238.
(57) Broström, M.; Nordin, A.; Pommer, L.; Branca, C.; Di Blasi, C. Influence of torrefaction on the devolatilization and oxidation kinetics of wood. *J. Anal. Appl. Pyrolysis* **2012**, *96*, 100−109.
(58) Biagini, E.; Tognotti, L. A generalized procedure for the devolatilization of biomass fuels based on the chemical components. *Energy Fuels* **2014**, *28*, 614−623.
(59) Hu, Q.; Yang, H.; Xu, H.; Wu, Z.; Lim, C. J.; Bi, X. T.; Chen, H. Thermal behavior and reaction kinetics analysis of pyrolysis and subsequent in-situ gasification of torrefied biomass pellets. *Energy Convers. Manage.* **2018**, *161*, 205−214.
(60) Antal, M. J., Jr.; Varhegyi, G. Cellulose Pyrolysis Kinetics: The Current State of Knowledge. *Ind. Eng. Chem. Res.* **1995**, *34*, 703−717.
(61) Branca, C.; Albano, A.; Di Blasi, C. Critical evaluation of global mechanisms of wood devolatilization. *Themochim. Acta* **2005**, *429*, 133−141.
(62) Coats, A. W.; Redfern, J. P. Kinetic parameters from thermogravimetric data. *Nature* **1964**, *201*, 68−69.
(63) Marsanich, K.; Barontini, F.; Cozzani, V.; Petarca, L. Advanced pulse calibration techniques for the quantitative analysis of TG-FTIR data. *Themochim. Acta* **2002**, *390*, 153−168.
(64) Li, J.; Zhang, X.; Pawlak-Kruczek, H.; Yang, W.; Kruczek, P.; Blasiak, W. Process simulation of co-firing torrefied biomass in a 220 MWe coal-fired power plant. *Energy Convers. Manage.* **2014**, *84*, 503−511.
(65) Biagini, E.; Barontini, F.; Tognotti, L. Devolatilization of biomass fuels and biomass components studied by TG/FTIR technique. *Ind. Eng. Chem. Res.* **2006**, *45*, 4486−4493.
(66) Di Blasi, C.; Branca, C.; Galgano, A.; Gallo, B. Role of Pretreatments in the Thermal Runaway of Hazelnut Shell Pyrolysis. *Energy Fuels* **2015**, *29*, 2514−2526.
(67) Gomez, C.; Velo, E.; Barontini, F.; Cozzani, V. Influence of Secondary Reactions on the Heat of Pyrolysis of Biomass. *Ind. Eng. Chem. Res.* **2009**, *48*, 10222−10233.
(68) Di Blasi, C. Modeling chemical and physical processes of wood and biomass pyrolysis. *Prog. Energy Combust. Sci.* **2008**, *34*, 47−90.
(69) Chen, W.-H.; Kuo, P.-C. A study on torrefaction of various biomass materials and its impact on lignocellulosic structure simulated by a thermogravimetry. *Energy* **2010**, *35*, 2580−2586.
(70) Chen, W.-H.; Kuo, P.-C. Torrefaction and co-torrefaction characterization of hemicellulose, cellulose and lignin as well as torrefaction of some basic constituents in biomass. *Energy* **2011**, *36*, 803−811.
(71) Collard, F.-X.; Blin, J. A review on pyrolysis of biomass constituents: Mechanisms and composition of the products obtained from the conversion of cellulose, hemicelluloses and lignin. *Renewable Sustainable Energy Rev.* **2014**, *38*, 594−608.
(72) Wang, S.; Dai, G.; Yang, H.; Luo, Z. Lignocellulosic biomass pyrolysis mechanism: A state-of-the-art review. *Prog. Energy Combust. Sci.* **2017**, *62*, 33−86.
(73) Ma, Z.; Chen, D.; Gu, J.; Bao, B.; Zhang, Q. Determination of pyrolysis characteristics and kinetics of palm kernel shell using TGA−FTIR and model-free integral methods. *Energy Convers. Manage.* **2015**, *89*, 251−259.
(74) Neves, D.; Thunman, H.; Matos, A.; Tarelho, L.; Gómez-Barea, A. Characterization and prediction of biomass pyrolysis products. *Prog. Energy Combust. Sci.* **2011**, *37*, 611−630.
(75) Di Blasi, C.; Signorelli, G.; Di Russo, C.; Rea, G. Product Distribution from Pyrolysis of Wood and Agricultural Residues. *Ind. Eng. Chem. Res.* **1999**, *38*, 2216−2224.

https://doi.org/10.1021/acsomega.1c02141
ACS Omega 2021, 6, 20264−20278